DOI: 10.1002/chem.200902543

Mechanism of the Asymmetric Autocatalytic Soai Reaction Studied by Density Functional Theory

Luca Schiaffino and Gianfranco Ercolani*[a]

Abstract: The mechanism of the Soai reaction has been thoroughly investigated at the M05-2X/6-31G(d) level of theory, by considering ten energetically distinct paths. The study indicates the fully enantioselective catalytic cycle of the homochiral dimers to be the dominant mechanism. Two other catalytic cycles are shown to both be important for correct understanding of the Soai reaction. These are the catalytic cycle of the heterochiral dimer and the non-enantioselective catalytic cycle of the homochiral dimers. The former has been proved to be not really competitive with the principal cycle, as required for the Soai reaction to manifest chiral amplification, whereas the latter, which is only slightly competitive with the principal one, nicely explains the experimental enantioselectivity observed in the reaction of 2-methylpyrimidine-5-carbaldehyde. The study has also evidenced the inadequacy of the B3LYP functional for mechanistic investigations of the Soai reaction.

Keywords: asymmetric amplification · autocatalysis · density functional calculations · reaction mechanisms · Soai reaction

Introduction

In spite of controversies about the origin of primordial symmetry breaking on prebiotic Earth, there is a general consensus that the initial tiny enantiomeric excess needed a mechanism of amplification to increase up to homochirality.[1] Such mechanisms are the object of intense investigation. To date the most successful processes are abrasive grinding of an initially racemic mixture of conglomerate crystals combined with fast solution racemization to obtain a single chiral solid phase;[2] spontaneous resolution by crystallization-induced asymmetric transformation;[3] and the Soai reaction,[4] consisting of the autocatalytic asymmetric addition of diisopropylzinc to pyrimidinyl aldehydes, for example, 2-methylpyrimidine-5-carbaldehyde (Scheme 1).

Although it occurs in a single homogeneous phase (i.e., the solution), the Soai reaction shows spectacular chiral amplification, triggered not only by added chiral inducers,[4] but also by optically active solvent impurities,[5] by an enantiomeric excess due to statistical fluctuations,[6] and lately by carbon-isotope chirality.[7] Owing to the strong bearing on the paradigms for the origin of homochirality in nature, there is great interest in the mechanism of the reaction.[8,9] From a kinetic analysis of the reaction of **1** in toluene at 25 °C, it was concluded that the homochiral dimers of **2** are the catalytically active species in statistical equilibrium with the catalytically inactive heterochiral dimer.[9a] Kinetic studies also showed that the reaction rate is first-order in the homochiral dimers, second-order in aldehyde, and independent of the concentration of iPr$_2$Zn.[9b] Homo- and heterochiral dimers, in statistical equilibrium with each other, were indeed evidenced by NMR spectroscopy at ambient temperature, and were shown to significantly associate with iPr$_2$Zn.[9c,g] Thus, in accordance with the observed zero-order rate in diisopropylzinc, the resting state at 25 °C is constituted by zinc-saturated dimers. With the help of these pieces of information and B3LYP/6-31G(d)//HF/3-21G(d) calcula-

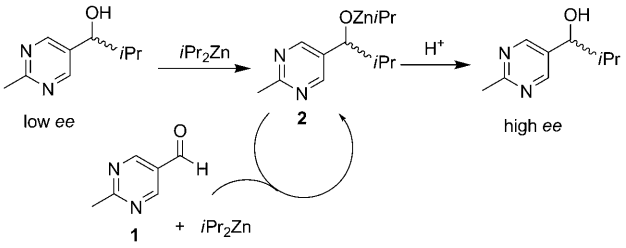

Scheme 1. Chiral amplification by the Soai autocatalytic reaction.

[a] Dr. L. Schiaffino, Prof. Dr. G. Ercolani
Dipartimento di Scienze e Tecnologie Chimiche
Università di Roma Tor Vergata
Via della Ricerca Scientifica, 00133 Roma (Italy)
Fax: (+39) 0672594328
E-mail: ercolani@uniroma2.it

Supporting information for this article is available on the WWW under http://dx.doi.org/10.1002/chem.200902543.

tions, we proposed the mechanism shown in Scheme 2, where R_2 and S_2 are the homochiral dimers; *RS* is the heterochiral dimer; Z is diisopropylzinc; $(R_2Z_2)^{I}$ and $(R_2Z_2)^{II}$, $(S_2Z_2)^{I}$ and $(S_2Z_2)^{II}$, and $(RSZ_2)^{I}$ and $(RSZ_2)^{II}$ are type I and type II constitutional isomers of zinc-saturated dimers; A is the aldehyde **1**, and the abbreviations of the remaining complexes are self-explanatory.[10]

The mechanism consists of fully enantioselective catalytic cycles driven by the homochiral dimer R_2 (left-hand side of Scheme 2) and its mirror image (right-hand side of Scheme 2). The two enantiomeric cycles are chemically connected through statistical equilibrations of homo- and heterochiral, as well as free and zinc-saturated, dimers. The catalytic cycle driven by the heterochiral dimer *RS* is not shown in Scheme 2 because it does not effectively compete with the two homochiral cycles.[10] Indeed, to observe chiral amplification it is required that the heterochiral dimer is significantly less reactive than the homochiral dimers. In this way the heterodimer acts like a trap that leaves the excess of the majority enantiomer as the dominant catalyst in solution.[11] For the sake of illustration, the homochiral "all-*R*" catalytic cycle is translated at the molecular level in Scheme 3, where the used nomenclature is explained below. To date this is the only mechanistic proposal for the Soai reaction detailed at the molecular level that is consistent with kinetic results and further corroborated by location and characterization of the transition states of the two irreversible steps.[10]

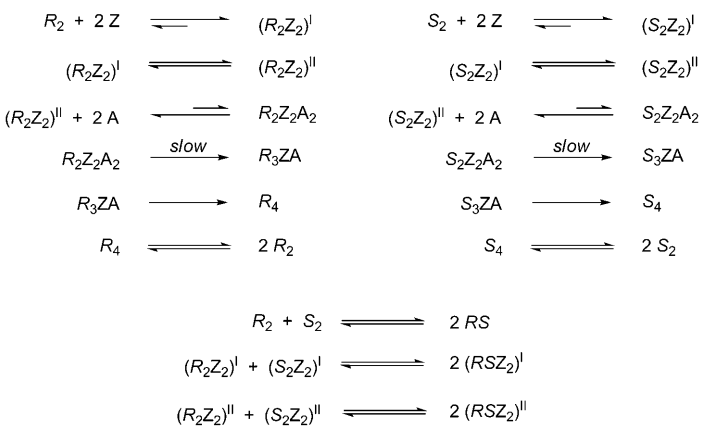

Scheme 2. Proposed mechanism for the Soai autocatalytic reaction.

The cycle begins with the dimer of **2**-*R*, that is, **3**-R_2, which binds two molecules of iPr$_2$Zn to yield the adduct **4**-R_2 [≡ $(R_2Z_2)^{I}$ in Scheme 2]. The latter undergoes isomerization to the active form of the catalyst **5**-R_2 [≡ $(R_2Z_2)^{II}$ in Scheme 2], which upon binding two molecules of aldehyde **1** yields **6**-*R,anti-R,anti-P* (≡ $R_2Z_2A_2$ in Scheme 2). The hexamolecular complex **6**-*R,anti-R,anti-P* evolves toward the rate-determining transition state, in which one of the two symmetrically equivalent Zn-bound isopropyl groups, for example, that encircled in the **6**-*R,anti-R,anti-P* structure, irreversibly attacks the aldehydic

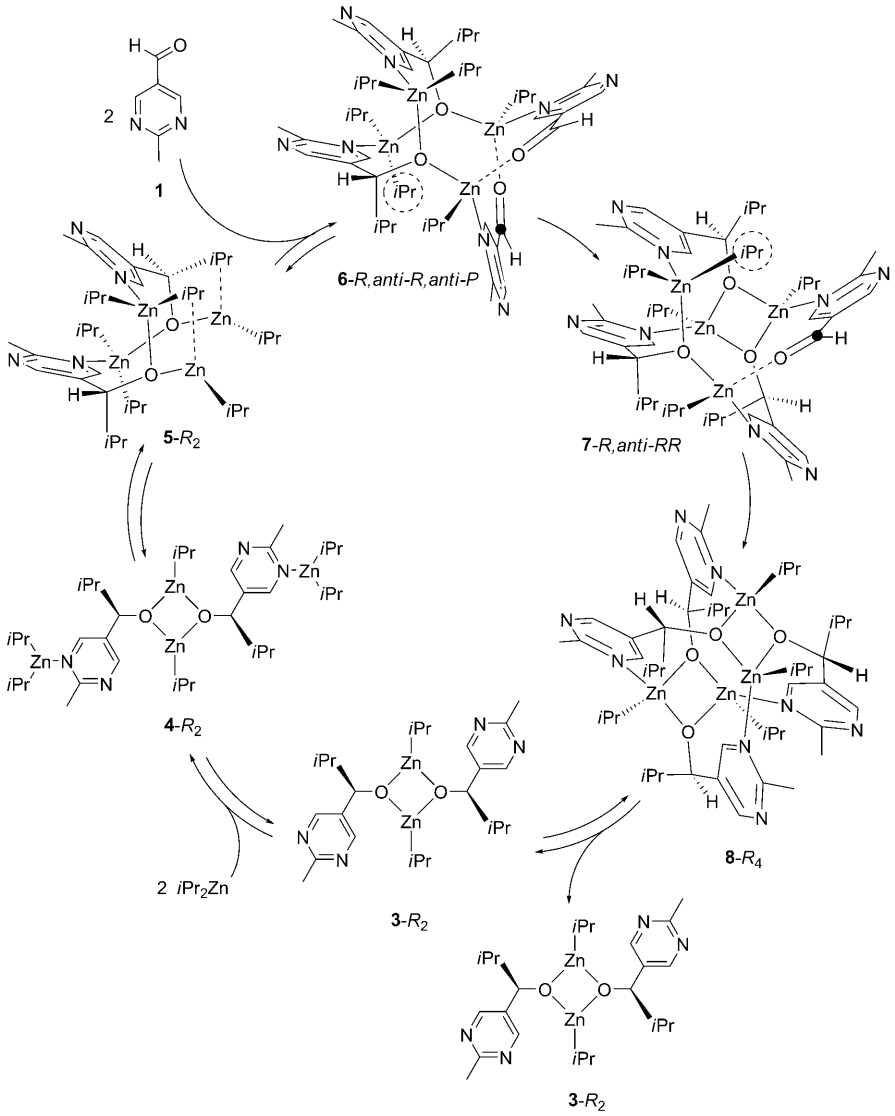

Scheme 3. Fully enantioselective catalytic cycle of the homochiral dimer **3**-R_2.

carbon next to it, marked by a large black dot, to yield, after interaction of the ex-aldehydic oxygen atom with the nearby zinc center, the pentamolecular complex **7**-*R,anti-RR* (≡ R_3ZA in Scheme 2). Fast and irreversible attack of the Zn-bound isopropyl group encircled in the **7**-*R,anti-RR* structure to the remaining aldehyde transforms the complex **7**-*R,anti-RR* into tetramer **8**-R_4. Finally, tetramer **8**-R_4 dissociates to yield two dimers **3**-R_2, each of which begins a new catalytic cycle. In the complex **6**-*R,anti-R,anti-P*, each of the isopropyl groups being transferred is correctly oriented to attack the *Re* face of the aldehyde, so that the addition product reproduces the chirality of the *R* catalyst acting as template.

Measurements by NMR spectroscopy showed that, while at 25 °C dimers are the most stable species, at low temperatures, for example, in the range from 0 to −25 °C, tetramers and higher oligomeric species become dominant.[9f,g] This fact has a profound influence on the extent of chiral amplification. Indeed, at 25 °C amplification of chirality is explained admirably well by considering dimers as the most stable species,[9b] whereas at low temperatures the observed amplifications are much larger. Since tetramers are the primary products of dimer aggregation, they should be the most important cause for the increased chiral amplification at low temperatures, possibly through a reservoir effect.[9e] We recently analyzed this proposal by carrying out a DFT study on diastereomers of barrel-like tetramers **8**.[12] The observed chiral amplifications were explained by suggesting that at low temperatures the resting state is mainly constituted by a mixture of rapidly equilibrating isomeric tetramers in which the heterochiral tetramer formed by dimerization of two **3**-*RS* units is the most stable among barrel-like tetramers.[12,13] Taking into account the caveat regarding the dependence of the nature of the resting state on temperature (dimeric or tetrameric), the mechanism detailed in Schemes 2 and 3 is well suited to explain the experimental results both at 25 °C and at lower temperatures. On deepening the study of the reaction, however, we realized that many more hexamolecular complexes of type **6** than those previously examined could form upon addition of two equivalents of aldehyde **1** to intermediates of type **5**, each of which has its own stereoselectivity. The overall stereoselectivity and chiral amplification of the reaction will ultimately depend on the relative energies of the rate-determining transition states transforming complexes **6** into complexes **7**. Thus, to validate our previously proposed mechanism, it is necessary to explore the reaction pattern of all possible isomeric complexes **6**. To reliably accomplish this task, higher level calculations are necessary. In this respect, we were attracted by the recent functional M05-2X developed by Zhao and Truhlar for systems in which main group thermochemistry, kinetics, and noncovalent interactions dominated by "medium-range" (≤5 Å) electron correlation are all important.[14,15] This functional was recently demonstrated to outperform the popular B3LYP functional in the energetic description of organic systems,[16] and is recommended as the most suitable one for accurate calculations of geometries and energetics of Zn compounds.[17] Accordingly, here we report a complete DFT study of the Soai reaction, examining the pathways of all possible isomeric complexes **6** with the M05-2X/6-31G(d) method. Some optimizations were also carried out with the B3LYP/6-31G(d) method for comparison purposes.

Results and Discussion

The previously proposed mechanism calculated with the M05-2X/6-31G(d) and B3LYP/6-31G(d) methods: Before exploring the reaction pattern of all possible isomeric complexes **6**, it is useful to illustrate the results of M05-2X/6-31G(d) and B3LYP/6-31G(d) geometry optimizations for the species characterizing the previously proposed mechanism, detailed in Schemes 2 and 3, including the transition states (TSs) of the two irreversible steps.[18] Relative gas-phase electronic energies are reported in Table 1. Figure 1 shows the energy diagram for the homochiral catalytic cycle illustrated in Scheme 3.

Table 1. Relative electronic energies [kcal mol^{-1}] of the species characterizing the previously proposed mechanism (Schemes 2 and 3) calculated in the gas phase with the M05-2X/6-31G(d) and B3LYP/6-31G(d) methods, and in the solution phase (toluene) with the single-point PCM-M05-2X/6-31G(d) method.[a]

Entry	Structure	M05-2X	B3LYP	PCM-M05-2X
1	**3**-R_2+2 *i*Pr$_2$Zn+2**1**	82.0	10.3	69.3
2	**4**-R_2+2**1**	44.5	−10.2	36.7
3	**5**-R_2+2**1**	24.5	−6.0	21.6
4	**6**-*R,anti-R,anti-P*	0.0	0.0	0.0
5	TS (**6**-*R,anti-R,anti-P*→**7**-*R,anti-RR*)	6.8	9.0	8.1
6	**7**-*R,anti-RR*	−61.0	−53.9	−59.4
7	TS (**7**-*R,anti-RR*→**8**-R_4)	−55.5	−44.4	−52.8
8	**8**-R_4	−131.8	−114.3	−129.2
9	2**3**-R_2	−67.2	−91.8	−73.6
10	**3**-*RS*+2 *i*Pr$_2$Zn+2**1**	82.7	10.0	71.1
11	**4**-*RS*+2**1**	45.0	−10.7	37.5
12	**5**-*RS*+2**1**	23.9	−6.7	21.0

[a] Not corrected for zero-point energy (ZPE).

There are no significant differences in the geometries calculated with the two methods, whereas energy differences are vast. The structure of intermediate **5**-R_2 featuring two isopropyl bridges with adjacent zinc atoms and the geometries of the TSs that have a rather early structure with slight elongation of the Zn–C bond relative to the *i*Pr group that is being transferred [M05-2X data indicate an elongation from 2.06 to 2.15 Å for TS (**6**-*R,anti-R,anti-P*→**7**-*R,anti-RR*), and from 2.06 to 2.13 Å for TS (**7**-*R,anti-RR*→**8**-R_4)] are noteworthy. The energy profiles depicted in Figure 1 span about 214 kcal mol^{-1} in the case of the M05-2X functional and about 124 kcal mol^{-1} in the case of the B3LYP functional. Such a large difference can be principally ascribed to the magnitude of the Zn–N and Zn–O interactions, which

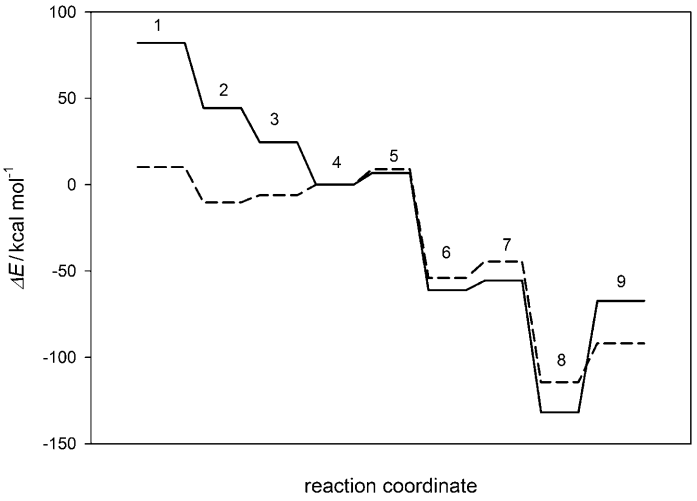

Figure 1. Energy diagram for the homochiral catalytic cycle (Scheme 3) computed in the gas phase with the M05-2X/6-31G(d) method (solid line) and the B3LYP/6-31G(d) method (dashed line). The numbers above the energy levels refer to the entries in Table 1.

appear to be much weaker when calculated with the B3LYP functional. Consider, for example, the interaction of **5**-R_2 with two aldehyde molecules to yield **6**-*R,anti-R,anti-P*; with the M05-2X functional this process is exothermic by 24.5 kcal mol^{-1}, whereas with the B3LYP functional it is endothermic by 6 kcal mol^{-1}. Which of the two functionals provides more realistic results? The magnitude of the interaction of **5**-R_2 with two aldehyde molecules seems particularly illuminating. An association that is endothermic in the gas phase, as suggested by B3LYP results, and that necessarily involves a large loss of entropy is expected to be highly endoergonic in solution. In contrast, this interaction appears to be only slightly endoergonic in solution under the conditions of the previously reported kinetic runs.[9b,19] Thus, the results obtained with the M05-2X functional in the gas phase appear to be more realistic.

In the light of the above results and the well-known deficiencies of the B3LYP method,[20] we conclude that such a functional is inadequate for computational studies on the Soai reaction. Since the M05-2X functional overcomes most of the shortcomings of the B3LYP functional,[14–17] the rest of the computations were performed with the M05-2X/6-31G(d) method only.

The Soai reaction is usually carried out in toluene or cumene. To evaluate the effect of toluene as solvent, relative energies were computed with the polarizable continuum model (PCM) by PCM-M05-2X/6-31G(d) single-point calculations on gas-phase M05-2X/6-31G(d) optimized geometries.[18,21] The results of such calculations are also reported in Table 1. Comparing the results obtained in toluene and in the gas phase with the M05-2X functional, it appears that solvent does not play a critical role, since the energy trend remains the same. Of course, energies obtained in solution without taking into account entropic effects cannot match the solution free-energy landscape. On the other hand, the aim of the present study was not to reproduce the solution behavior but to evidence the relevant intermediates and TSs, and verify that the relative energies of the latter are compatible with the stereoselectivity and chiral amplification observed in the Soai reaction. Accordingly, in the following only gas-phase results are considered.

To complete the energetic description of the species appearing in Scheme 2, besides the two homochiral cycles we must also take into account the metathesis equilibria between homo- and heterochiral, as well as free and zinc-saturated, dimers. Comparing entries 1–3 in Table 1 with the corresponding entries 10–12, it appears that the homochiral dimers have the same energy as the corresponding heterochiral dimers within 0.7 kcal mol^{-1} or less at both the M05-2X/6-31G(d) and B3LYP/6-31G(d) levels. Such energy differences are not significant, because they are largely within the expected errors of the above computational methods. Thus, homochiral dimers and the corresponding heterochiral dimers have practically the same energy, in agreement with kinetic[9a] and ^{1}H NMR[9c] studies in solution showing that the metathesis equilibria between homo- and heterochiral dimers are only governed by statistics. In this case the accordance between the M05-2X/6-31G(d) and B3LYP/6-31G(d) results is not surprising because the metathesis equilibria do not involve any change of zinc coordination.

Classification of hexamolecular complexes and evaluation of their stability: To understand the structures of all the possible hexamolecular complexes of type **6**, it is useful to briefly review the structures of all stereoisomers of barrel-like tetramers **8**.[12] There are seven stereoisomers of type **8**, whose structure is best understood by considering them as the products of dimerization of dimers of type **3**. Consider the process of dimer dimerization as occurring by the reciprocal coordination of the zinc atoms of one of the dimers by the nitrogen atoms of the other. Chiral **8**-R_4 is formed from two **3**-R_2 units (its enantiomer is **8**-S_4), chiral **8**-R_3S from one **3**-R_2 and one **3**-*RS* unit (its enantiomer is **8**-S_3R), chiral **8**-$(RS)_2$-*P* from two **3**-*RS* units arranged according to an axially chiral *P* configuration (its enantiomer is **8**-$(RS)_2$-*M*), and achiral **8**-R_2S_2 (S_4 symmetry) from one **3**-R_2 and one **3**-S_2 unit. In total there are four diastereomeric structures of different energy, namely, **8**-R_4, **8**-R_3S, **8**-$(RS)_2$-*P*, and **8**-R_2S_2.[12] The asymmetric carbon atoms of tetramers **8** occupy the vertices of an elongated tetrahedron, as shown in Figure 2 for the case of **8**-R_4. Viewing such tetrahedra along the AB axis from the A end gives the corresponding Fischer projections of the structures, as shown in Figure 2.

Complexes **6** are the precursors of tetramers **8**; they are obtained by retrosynthetic transformation of two chiral units of **8**, one on the front and one on the back, into the corresponding precursors, that is, aldehyde **1** and *i*Pr$_2$Zn, properly placed with respect to each other to give the correct configuration of the chiral unit upon reaction. For simplicity let us consider two front chiral units, that is, those appearing on the horizontal line of the Fischer projection, with the same configuration, say *R*–*R*, and let us transform one of the two

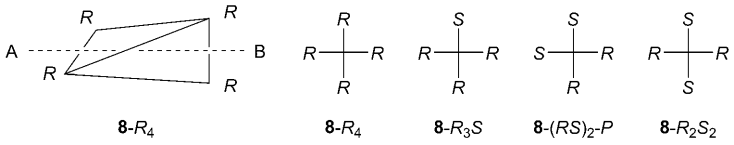

Figure 2. Structure **8**-R_4 schematically represented on the left as an elongated tetrahedron. Viewed along the AB axis from the A end, the structure appears as the corresponding Fischer projection on the right. The other Fischer projections represent the diastereomers **8**-R_3S, **8**-$(RS)_2$-P, and **8**-R_2S_2.

units into the aldehyde **1** and iPr$_2$Zn. For the iPr$_2$Zn moiety to be correctly oriented to attack the *Re* face of the aldehyde, it must be positioned as shown in the structure dubbed *anti* in Figure 3. This notation refers to the orientation of the Zn atom of the iPr$_2$Zn moiety relative to the isopropyl group bound to the *R* carbon atom, as emphasized by the bond torsion in bold. In the *anti* arrangement the aldehyde is predisposed to reproduce the chirality of the catalyst acting as template, and thus the arrangement shown in Figure 3 can be dubbed "*R,anti*". This arrangement can be easily recognized in the structure of **6**-*R,anti-R,anti-P* in Scheme 3. To represent this arrangement on a Fischer projection we denote the aldehyde predisposed to yield an *R* chiral unit as A_R.

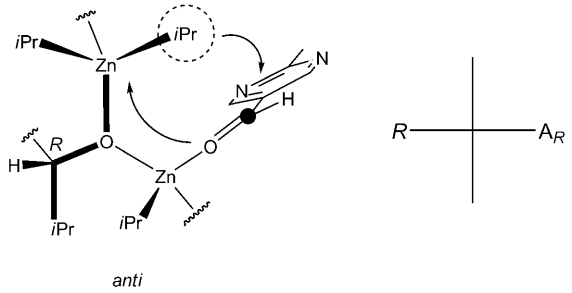

Figure 3. Left: frontal portion of a complex of type **6** in the *anti* arrangement. In this arrangement the iPr$_2$Zn moiety is correctly oriented to attack the *Re* face of the aldehyde so as to reproduce the chirality of the *R* catalyst acting as template. On the right it is shown how this arrangement can be schematized in a Fischer projection.

Let us consider now the case in which the two front chiral units have a different configuration, say *R*–*S*, and let us transform the unit on the right into the aldehyde **1** and iPr$_2$Zn. For the iPr$_2$Zn moiety to be oriented to attack the *Si* face of the aldehyde, it must be positioned as shown in the structure dubbed *syn* in Figure 4. In the *syn* arrangement the aldehyde is predisposed to yield a configuration opposite to that of the catalyst. Accordingly, the arrangement shown in Figure 4 can be dubbed "*R,syn*".

This arrangement is represented on a Fischer projection in Figure 4. Note that the terms *anti* and *syn* refer to the relative predisposition of the aldehyde with respect to the configuration of the neighboring chiral unit **2** acting as template. Thus, the mirror images of the arrangements in Figures 3 and 4 are dubbed "*S,anti*" and "*S,syn*", respectively.

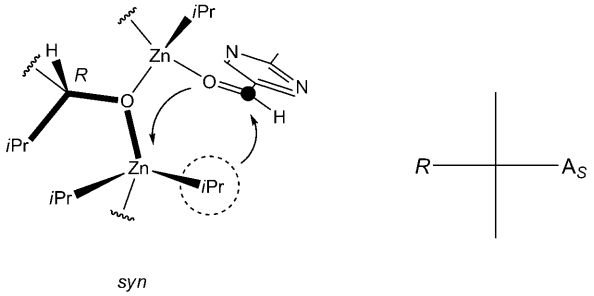

Figure 4. Left: frontal portion of a complex of type **6** in the *syn* arrangement. In this arrangement the iPr$_2$Zn moiety is oriented to attack the *Si* face of the aldehyde so as to yield a configuration opposite to that of the *R* catalyst. On the right it is shown how this arrangement can be schematized in a Fischer projection.

Of course an identical notation can be applied upon transformation of one of the two back chiral units, that is, those appearing on the vertical line of the Fischer projection. Accordingly, all hexamolecular complexes **6** as precursors of diastereomeric tetramers **8** are shown schematically in Figure 5.

The name of each complex **6**, reported below the Fischer projection, is built up by listing the horizontal and vertical arrangements (note that interchange of the labels does not alter the structure; for example, *R,anti-S,syn* is equivalent to *S,syn-R,anti*) followed by the helical descriptor *P* or *M*. The latter indicates the relative position of the front and back aldehydes, and is assigned through rotation of the front aldehyde in the direction to the back aldehyde. The descriptor *P* denotes clockwise rotation, and *M* counterclockwise rotation. Some comments on the complexes **6** in Figure 5 are in order here. It is tempting to consider the various structures as diastereomers of each other. This is not always true; for example, comparing the structures **6**-*R,anti-R,anti-P* and **6**-*R,anti-R,anti-M*, it appears that in the former each iPr$_2$Zn moiety is coordinated by the pyrimidine ring belonging to a **2**-*R* unit, whereas in the latter each iPr$_2$Zn moiety is coordinated by the pyrimidine ring belonging to an aldehydic unit **1**. Thus the two structures do not represent two diastereomers but two constitutional isomers. Moreover, two structures, namely **6**-*R,anti-S,anti-P* and **6**-*R,anti-S,anti-M*, are enantiomers of each other; they are the precursors of the achiral *meso* form **8**-R_2S_2. In contrast to **8**-R_2S_2, all other diastereomeric tetramers **8** in the upper row of Figure 4 are chiral, and the corresponding enantiomers have as precursors the enantiomers of complexes **6** shown in the corresponding columns of Figure 5. In conclusion there are ten chiral hexamolecular complexes of type **6** of different energy, that is, all those shown in Figure 5 with the exclusion of **6**-*R,anti-S,anti-M*, which is the mirror image of **6**-*R,anti-S,anti-P*.[22] Each of these complexes has a distinct mirror image; thus, in total there are 20 hexamolecular complexes of type **6**. This means that in principle there are 20 distinct catalytic cycles in competition with each other, half of which

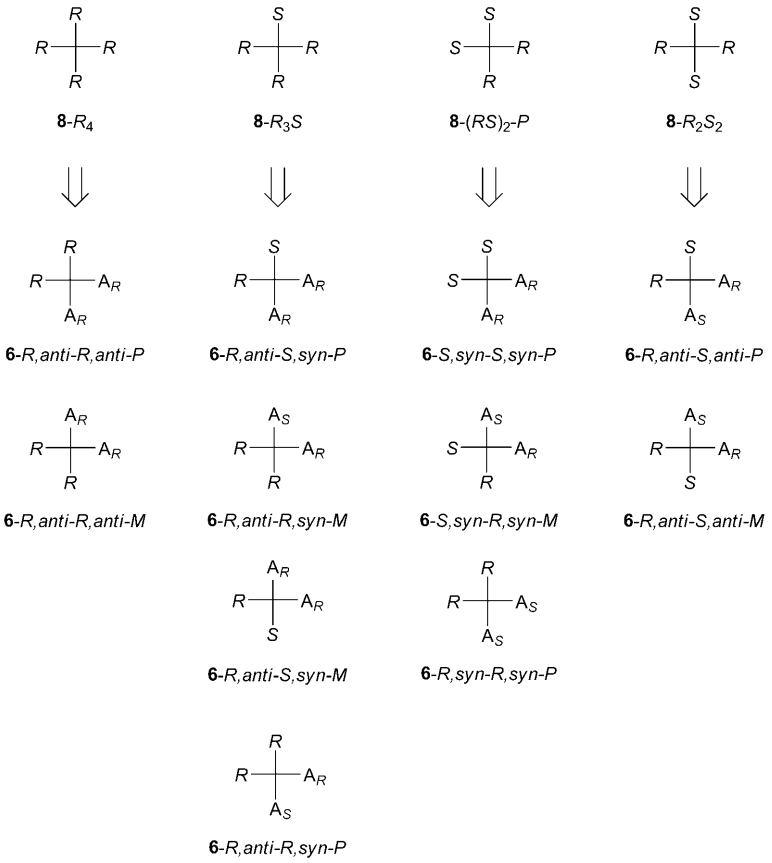

Figure 5. Hexamolecular complexes **6** obtained retrosynthetically from the diastereomeric tetramers **8** in the top row.

are mirror images of the other half. One of these cycles, namely, that pertaining to the formation of the hexamolecular complex **6**-*R,anti-R,anti-P*,is illustrated in Scheme 3, and the results of the corresponding calculations are shown in Table 1 and Figure 1. We carried out geometry optimizations with the M05-2X/6-31G(d) method on all the remaining nine chiral hexamolecular complexes of type **6** with distinct energy;[18] the optimized structures are shown in Figure 6 and their relative electronic energies are reported in Table 2.

It is not easy to explain the different energies in Table 2 on the basis of the obtained structures, because a number of interactions play a role, including aromatic–aromatic stacking, steric,[23] and coordination of zinc by the pyrimidinyl ring of either **1** or **2** moieties, the former being a worse donor than the latter because of the electron-withdrawing effect of the formyl group.

To determine whether the homochiral catalytic cycle reported in Scheme 3 has any serious competitor among the remaining nine distinct catalytic cycles originating from complexes **6** in Table 2, we need to compare the energies of the rate-determining TSs transforming complexes **6** into complexes **7**.

Evaluation of the relative energies of the rate-determining transition states: Before discussing the energies of the TSs,

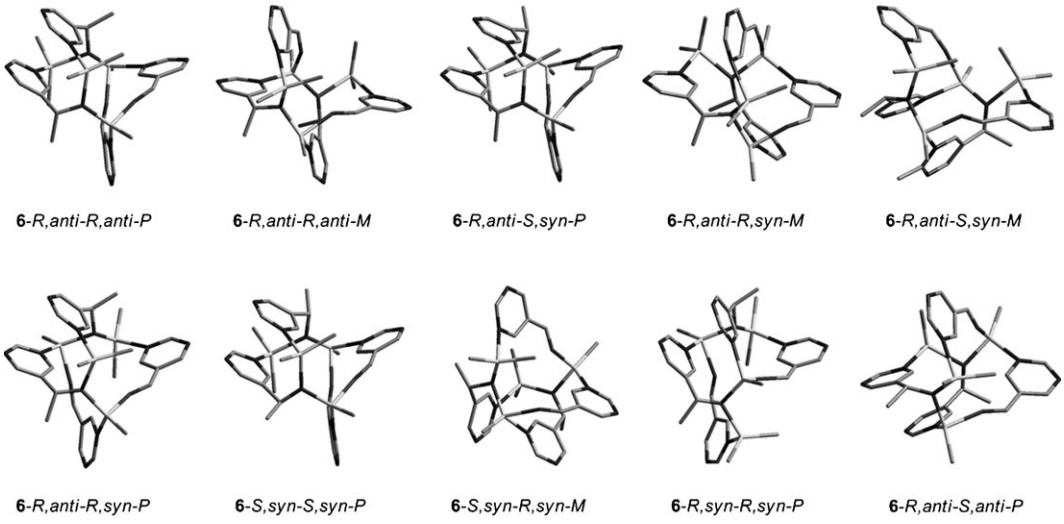

Figure 6. M05-2X/6-31G(d) optimized geometries of the ten chiral hexamolecular complexes of type **6** of different energy. Methyl groups and hydrogen atoms have been omitted for clarity.

Table 2. M05-2X/6-31G(d) relative electronic energies of the ten chiral hexamolecular complexes of type **6** with distinct energy.[a]

Entry	Structure	ΔE [kcal mol^{-1}]
1	**6**-*R,anti-R,anti-P*	0.0
2	**6**-*R,anti-R,anti-M*	5.7
3	**6**-*R,anti-S,syn-P*	2.9
4	**6**-*R,anti-R,syn-M*	9.8
5	**6**-*R,anti-S,syn-M*	12.6
6	**6**-*R,anti-R,syn-P*	1.4
7	**6**-*S,syn-S,syn-P*	6.9
8	**6**-*S,syn-R,syn-M*	14.1
9	**6**-*R,syn-R,syn-P*	3.5
10	**6**-*R,anti-S,anti-P*	7.8

[a] Not corrected for ZPE.

Table 3. M05-2X/6-31G(d) relative electronic energies of the TSs between some of the complexes **6** in Table 2 (entries 1, 2, 3, 6, 7, 9) and the corresponding complexes **7**.[a,b]

Entry	Structure	ΔE [kcal mol^{-1}]
1[c]	TS (**6**-*R,anti-R,anti-P*→**7**-*R,anti-RR*)	6.8
2	TS (**6**-*R,anti-R,anti-M*→**7**-*R,anti-RR*)	17.1
3	TS (**6**-*R,anti-S,syn-P*→**7**-*S,syn-RR*)	14.4
4	TS (**6**-*R,anti-S,syn-P*→**7**-*R,anti-SR*)	9.0
5	TS (**6**-*R,anti-R,syn-P*→**7**-*R,syn-RR*)	9.7
6	TS (**6**-*R,anti-R,syn-P*→**7**-*R,anti-RS*)	8.5
7	TS (**6**-*S,syn-S,syn-P*→**7**-*S,syn-SR*)	12.0
8	TS (**6**-*R,syn-R,syn-P*→**7**-*R,syn-RS*)	14.2

[a] Not corrected for ZPE. [b] Energies are relative to that of **6**-*R,anti-R,anti-P*. [c] Coincident with entry 5 of Table 1.

it is necessary to establish a nomenclature for complexes **7**. Such complexes consist of an *i*Pr_2Zn molecule, an aldehyde molecule **1**, and three molecules of **2**, each with its own stereochemistry. We can continue to use the approach of Fischer projections by placing the unreacted aldehyde with its own chiral predisposition to the right of the horizontal line of the Fischer projection. The name of the structure is built by listing the horizontal and vertical arrangements, listing the chirality of the two units of **2** on the vertical line from top to bottom. For example the name of the Fischer projection shown in Figure 7 is **7**-*R,anti-SR*.

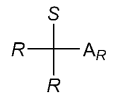

7-*R,anti-SR*

Figure 7. An example of the Fischer projection used to describe the structure of a complex of type **7**. The unreacted aldehyde is placed to the right of the horizontal line. The name is built by listing the horizontal and vertical arrangements, listing the chirality of the two units of **2** on the vertical line from top to bottom.

With regard to the energies of the TSs, some of the catalytic cycles can be excluded without actually doing the calculations. The energy of the rate-determining TS of the catalytic cycle reported in Scheme 3 (entry 5 in Table 1) is 6.8 kcal mol^{-1}. Some of the complexes in Table 2 have an energy greater than this value by not less than 1 kcal mol^{-1}. Considering that, on going toward the TS, the energy must necessarily further increase, we can safely exclude the complexes relative to entries 4, 5, 8, 10 from the competition. Accordingly, we have located and fully characterized by frequency calculations all the TSs between the remaining complexes **6** in Table 2 (entries 1, 2, 3, 6, 7, 9) and the corresponding complexes **7**;[18] their relative electronic energies are reported in Table 3.

Note that the complexes relative to entries 1, 2, 7, and 9 in Table 2 present the same arrangement on the front and on the back; they are symmetric and give rise to a single TS no matter which of the two aldehydes reacts. The corresponding TSs are those relative to entries 1, 2, 7, and 8 in Table 3. In contrast the complexes relative to entries 3 and 6 in Table 2 are unsymmetric, and each of the two complexes gives rise to two distinct TSs depending whether the reaction involves the front or the back aldehyde. The TSs corresponding to entry 3 in Table 2 are those relative to entries 3 and 4 in Table 3; the TSs corresponding to entry 6 in Table 2 are those relative to entries 5 and 6 in Table 3.

Gratifyingly, the rate-determining TS of the homochiral catalytic cycle shown in Scheme 3 has the lowest energy (Table 3, entry 1) in agreement with our previous conclusion that this catalytic cycle is the most important for the outcome of the Soai reaction.[10] However, there are two other TSs that are worth discussing since they are only 2.2 (Table 3, entry 4) and 1.7 kcal mol^{-1} (Table 3, entry 6) higher in energy than the lowest energy TS. The two TSs characterize two catalytic cycles that were not previously considered.[24]

Let us consider the catalytic cycle characterized by the TS of entry 4 in Table 3, illustrated in Scheme 4. We have dubbed this cycle the "*R*-bent" catalytic cycle of the heterochiral dimer, because although the free and zinc-saturated heterodimers are *meso* forms, the other species are chiral, and the cycle produces homochiral dimer **3**-R_2. Of course, the mirror image of this cycle, namely, the "*S*-bent" catalytic cycle, will produce the same quantity of homochiral dimer **3**-S_2. The two homodimers are in rapid equilibration with the heterodimer, and thus the combined action of the two enantiomeric cycles leads to reproduction of the heterodimer. In the Introduction we remarked that to observe chiral amplification it is required that the heterochiral dimer is significantly less reactive than the homochiral dimers, the rate of increase of *ee* with respect to conversion being at its maximum when the reactivity of the heterodimer is negligible with respect to that of the homodimers. A difference of 2.2 kcal mol^{-1} between the TSs implies that the heterodimer is 41 times less reactive than the homodimers at 25 °C. This factor is more than sufficient to assure rapid amplification of chirality in the Soai reaction.

Let us consider now the catalytic cycle characterized by the TS of entry 6, illustrated in Scheme 5. In this cycle the homodimeric catalyst **3**-R_2 displays the "wrong" selectivity because, instead of reproducing itself as in the cycle of Scheme 3, it catalyzes formation of heterochiral dimer **3**-*RS*. The cycle does not show any preference for either of the two enantiomers of **2** and thus must be considered to be non-enantioselective. The overall enantioselectivity of homochiral catalyst **3**-R_2 will depend on the relative impor-

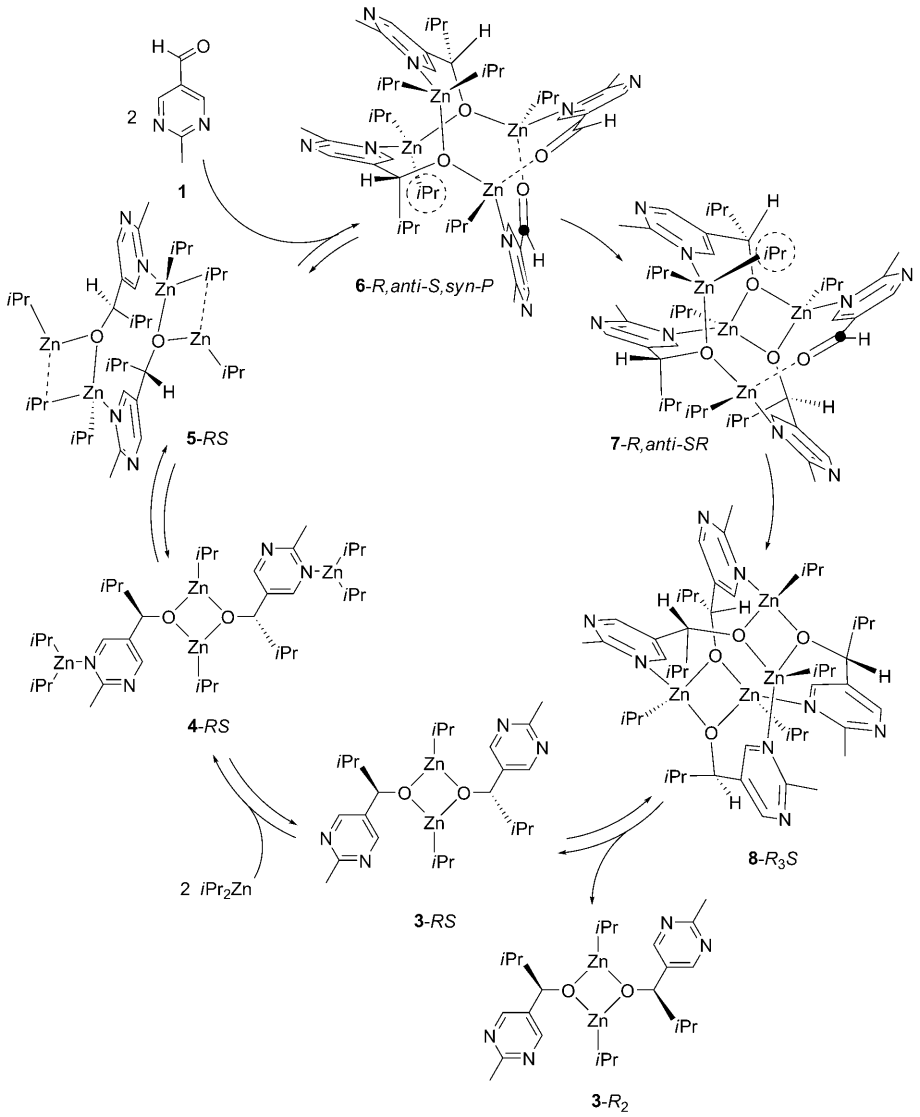

Scheme 4. "*R*-bent" catalytic cycle of heterochiral dimer **3**-*RS*.

tance of the cycles shown in Schemes 3 and 5. In previous work we faced the problem of the enantioselectivity of the catalyst in the Soai reaction.[12] We defined the enantioselectivity constant $k_{es}=(k_{ret}-k_{inv})/(k_{ret}+k_{inv})$ spanning the range from 0 to 1, where the rate constants k_{ret} and k_{inv} refer to the processes of chiral retention (strict autocatalysis) and chiral inversion (enantiocatalysis), in which the substrate A is converted to a product having, respectively, the same and the opposite configuration as the catalyst. In the case of the Soai reaction with substrate **1**, the experimental value of k_{es}, determined on the basis of the limit value of *ee*, was 0.96.[12] Defining the rate constants for the fully enantioselective (Scheme 3) and the non-enantioselective (Scheme 5) catalytic cycles as $k_{100\%}$ and $k_{0\%}$, respectively, it follows that $k_{ret}=2k_{100\%}+k_{0\%}$, because two molecules of **2**-*R* are produced in the fully enantioselective cycle and one molecule of **2**-*R* in the non-enantioselective cycle, whereas $k_{inv}=k_{0\%}$, because only one molecule of **2**-*S* is produced in the non-enantioselective cycle. Accordingly, the enantioselectivity constant becomes $k_{es}=(k_{100\%}/k_{0\%})/[(k_{100\%}/k_{0\%})+1]$. A difference of 1.7 kcal mol^{-1} between the TSs of the two cycles implies that $k_{100\%}/k_{0\%}=18$ at 25 °C, giving $k_{es}=0.95$, in surprisingly good agreement with the experimental result.

Conclusion

The mechanism of the Soai reaction previously proposed by us in a preliminary communication[10] has been thoroughly investigated with the recently developed M05-2X functional and 6-31G(d) basis set. This computational method has been recommended for the accurate energetic description of organic compounds containing zinc.[17] Eight new catalytic cycles with distinct energetics were investigated, besides the two previously investigated at the B3LYP/6-31G(d)//HF/3-21G(d) level of theory.[10] The present study confirms that the dominant mechanism of the Soai reaction is that based on the previously proposed homochiral cycle, sketched in Scheme 2 and translated at the molecular level in Scheme 3. However, this study has also evidenced that two other catalytic cycles, not previously considered, are both important for correct understanding of the Soai reaction. These are the catalytic cycle of the heterochiral dimer, illustrated in Scheme 4, and the non-enantioselective catalytic cycle of the homochiral dimers, illustrated in Scheme 5. The former proved to be not really competitive with the principal cycle, as required for the Soai reaction to manifest chiral amplification, whereas the latter, which is only slightly competitive with the principal cycle, nicely explains the experimental enantioselectivity observed in the Soai reaction with substrate **1**. The study has also promoted the use of the M05-2X functional for the study of the Soai reaction by evidencing the inadequacy of the B3LYP functional to produce sensible results.

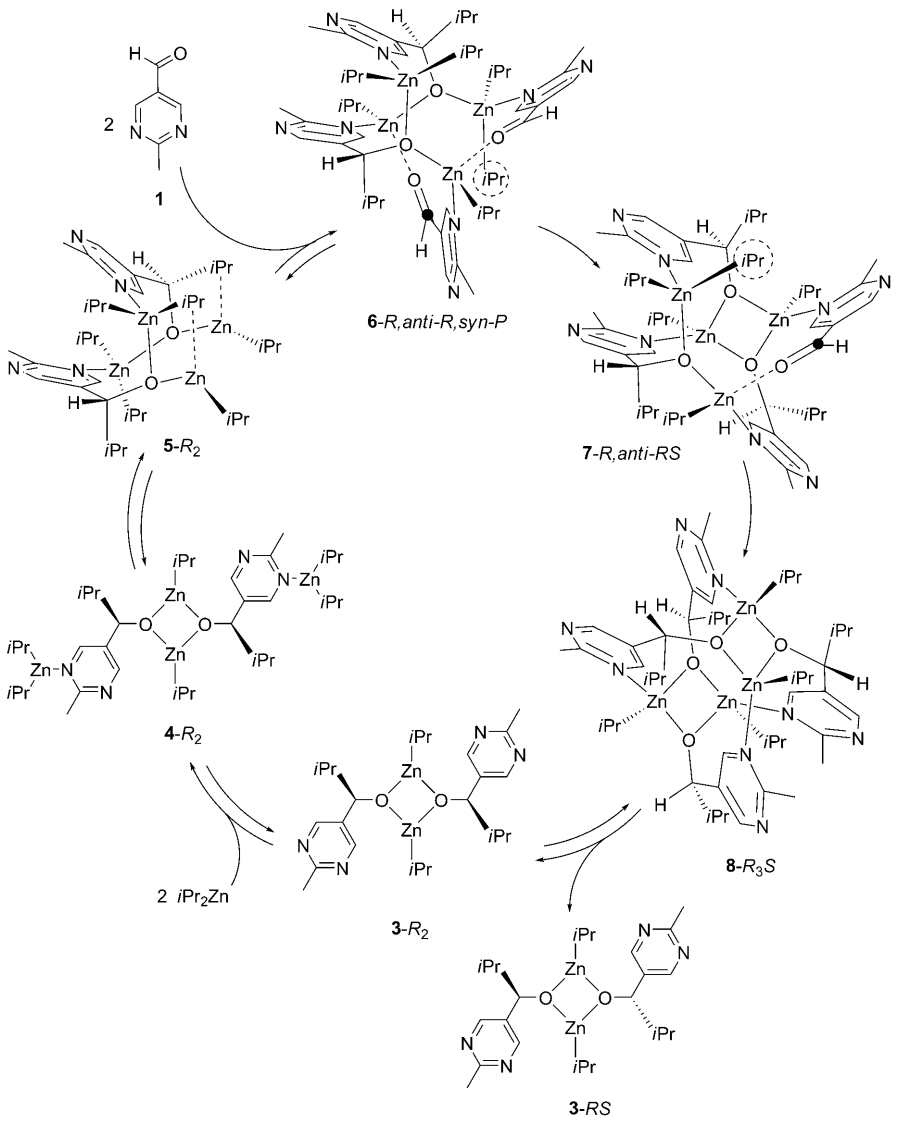

Scheme 5. Non-enantioselective catalytic cycle of homochiral dimer **3**-R_2.

[1] a) B. L. Feringa, R. A. van Delden, *Angew. Chem.* **1999**, *111*, 3624–3645; *Angew. Chem. Int. Ed.* **1999**, *38*, 3418–3438; b) U. Meierhenrich, *Amino Acids and the Asymmetry of Life*, Springer, Berlin, **2008**; c) A. Guijarro, M. Yus, *The Origin of Chirality in the Molecules of Life*, RSC, Cambridge, **2009**.

[2] a) C. Viedma, *Phys. Rev. Lett.* **2005**, *94*, 065504; b) C. Viedma, *Astrobiology* **2007**, *7*, 312–319; c) W. L. Noorduin, T. Izumi, A. Millemaggi, M. Leeman, H. Meekes, W. J. P. van Enckevort, R. M. Kellogg, B. Kaptein, E. Vlieg, D. G. Blackmond, *J. Am. Chem. Soc.* **2008**, *130*, 1158–1159; d) W. L. Noorduin, H. Meekes, W. J. P. van Enckevort, A. Millemaggi, M. Leeman, B. Kaptein, R. M. Kellogg, E. Vlieg, *Angew. Chem.* **2008**, *120*, 6545–6547; *Angew. Chem. Int. Ed.* **2008**, *47*, 6445–6447; e) B. Kaptein, W. L. Noorduin, H. Meekes, W. J. P. van Enckevort, R. M. Kellogg, E. Vlieg, *Angew. Chem.* **2008**, *120*, 7336–7339; *Angew. Chem. Int. Ed.* **2008**, *47*, 7226–7229; f) C. Viedma, J. E. Ortiz, T. de Torres, T. Izumi, D. G. Blackmond, *J. Am. Chem. Soc.* **2008**, *130*, 15274–15275; g) S. B. Tsogoeva, S. Wei, M. Freund, M. Mauksch, *Angew. Chem.* **2009**, *121*, 598–602; *Angew. Chem. Int. Ed.* **2009**, *48*, 590–594; h) W. L. Noorduin, P. van der Asdonk, H. Meekes, W. J. P. van Enckevort, B. Kaptein, M. Leeman, R. M. Kellogg, E. Vlieg, *Angew. Chem.* **2009**, *121*, 3328–3330; *Angew. Chem. Int. Ed.* **2009**, *48*, 3278–3280; i) W. L. Noorduin, B. Kaptein, H. Meekes, W. J. P. van Enckevort, R. M. Kellogg, E. Vlieg, *Angew. Chem.* **2009**, *121*, 4651–4653; *Angew. Chem. Int. Ed.* **2009**, *48*, 4581–4583.

[3] a) M. Håkansson, M. Vestergren, B. Gustafsson, G. Hilmersson, *Angew. Chem.* **1999**, *111*, 2336–2338; *Angew. Chem. Int. Ed.* **1999**, *38*, 2199–2201; b) A. Lennartson, M. Vestergren, M. Håkansson, *Chem. Eur. J.* **2005**, *11*, 1757–1762; c) A. Lennartson, M. Håkansson, *Angew. Chem.* **2009**, *121*, 5983–5985; *Angew. Chem. Int. Ed.* **2009**, *48*, 5869–5871; d) A. Pettersen, A. Lennartson, M. Håkansson, *Organometallics* **2009**, *28* , 3567–3569.

[4] a) K. Soai, T. Shibata, H. Morioka, K. Choji, *Nature* **1995**, *378*, 767–768; b) K. Soai, T. Shibata, I. Sato, *Acc. Chem. Res.* **2000**, *33*, 382–390; c) K. Soai, T. Kawasaki, *Chirality* **2006**, *18*, 469–478; d) K. Soai, T. Kawasaki, *Top. Curr. Chem.* **2008**, *271–274*, 1–33.

[5] D. A. Singleton, L. K. Vo, *J. Am. Chem. Soc.* **2002**, *124*, 10010–10011.

[6] a) Patent: K. Soai, T. Shibata, Y. Kowata, JP-Kokai 9-268179, **1997**; b) K. Soai, I. Sato, T. Shibata, S. Komiya, M. Hayashi, Y. Matsueda, H. Imamura, T. Hayase, H. Morioka, H. Tabira, J. Yamamoto, Y Kowata, *Tetrahedron: Asymmetry* **2003**, *14*, 185–188; c) I. D. Gridnev, J. M. Serafimov, H. Quiney, J. M. Brown, *Org. Biomol. Chem.* **2003**, *1*, 3811–3819; d) B. Barabas, L. Caglioti, C. Zucchi, M. Maioli, E. Gál, K. Micskei, G. Pályi, *J. Phys. Chem. B* **2007**, *111*, 11506–11510.

[7] a) T. Kawasaki, Y. Matsumura, T. Tsutsumi, K. Suzuki, M. Ito, K. Soai, *Science* **2009**, *324*, 492–495; b) T. Kawasaki, M. Shimizu, D. Nishiyama, M. Ito, H. Ozawa, K. Soai, *Chem. Commun.* **2009**, 4396–4398.

[8] a) I. Sato, D. Omiya, K. Tsukiyama, Y. Ogi, K. Soai, *Tetrahedron: Asymmetry* **2001**, *12*, 1965–1969; b) I. Sato, D. Omiya, H. Igarashi, K. Kato, Y. Ogi, K. Tsukiyama, K. Soai, *Tetrahedron: Asymmetry* **2003**, *14*, 975–979; c) T. Buhse, *Tetrahedron: Asymmetry* **2003**, *14*, 1055–1061; d) J. Rivera Islas, D. Lavabre, J.-M. Grevy, R. Hernandez Lamoneda, H. Rojas Cabrera, J.-C. Micheau, T. Buhse, *Proc. Natl. Acad. Sci. USA* **2005**, *102*, 13743–13748; e) Y. Saito, H. Hyuga, *J. Phys. Soc. Jpn.* **2004**, *73*, 33–35; f) Y. Saito, H. Hyuga, *J. Phys. Soc. Jpn.* **2004**, *73*, 1685–1688; g) J. Crusats, D. Hochberg, A. Moyano, J. M. Ribó, *ChemPhysChem* **2009**, *10*, 2123–2131.

[9] a) D. G. Blackmond, C. R. McMillan, S. Ramdeehul, A. Schorm, J. M. Brown, *J. Am. Chem. Soc.* **2001**, *123*, 10103–10104; b) F. G. Buono, D. G. Blackmond, *J. Am. Chem. Soc.* **2003**, *125*, 8978–8979; c) I. D. Gridnev, J. M. Serafimov, J. M. Brown, *Angew. Chem.* **2004**, *116*, 4992–4995; *Angew. Chem. Int. Ed.* **2004**, *43*, 4884–4887; d) I. D. Gridnev, J. M. Brown, *Proc. Natl. Acad. Sci. USA* **2004**, *101*, 5727–5731; e) I. D. Gridnev, *Chem. Lett.* **2006**, *35*, 148–153; f) J. Klankermayer, I. D. Gridnev, J. M. Brown, *Chem. Commun.* **2007**,

3151–3153; g) J. M. Brown, I. D. Gridnev, J. Klankermayer, *Top. Curr. Chem.* **2008**, *271–274*, 35–65.
[10] L. Schiaffino, G. Ercolani, *Angew. Chem.* **2008**, *120*, 6938–6941; *Angew. Chem. Int. Ed.* **2008**, *47*, 6832–6835.
[11] The importance of hetero versus homochiral dimers for nonlinear effects in organozinc additions has been intensively investigated, both experimentally and computationally: a) M. Kitamura, S. Suga, M. Niwa, R. Noyori, *J. Am. Chem. Soc.* **1995**, *117*, 4832–4842; b) M. Yamakawa, R. Noyori, *J. Am. Chem. Soc.* **1995**, *117*, 6327–6335; c) M. Kitamura, S. Suga, H. Oka, R. Noyori, *J. Am. Chem. Soc.* **1998**, *120*, 9800–9809; d) C. Girard, H. B. Kagan, *Angew. Chem.* **1998**, *110*, 3088–3127; *Angew. Chem. Int. Ed.* **1998**, *37*, 2922–2959; e) M. Yamakawa, R. Noyori, *Organometallics* **1999**, *18*, 128–133; f) B. Goldfuss, M. Steigelmann, S. I. Khan, K. N. Houk, *J. Org. Chem.* **2000**, *65*, 77–82; g) B. Goldfuss, M. Steigelmann, F. Rominger, *Eur. J. Org. Chem.* **2000**, 1785–1792; h) M. Steigelmann, Y. Nisar, F. Rominger, B. Goldfuss, *Chem. Eur. J.* **2002**, *8*, 5211–5218; i) T. Satyanarayana, S. Abraham, H. B. Kagan, *Angew. Chem.* **2009**, *121*, 464–503; *Angew. Chem. Int. Ed.* **2009**, *48*, 456–494.
[12] L. Schiaffino, G. Ercolani, *ChemPhysChem* **2009**, *10*, 2508–2515.
[13] A cautionary note is in order here, since new accurate experimental results regarding the reaction of 2-(1-adamantylethynyl)-pyrimidine-5-carbaldehyde, published by Gehring et al. while ref. [12] was in press, could lead to a re-evaluation of the nature of the resting state in the Soai reaction as a function of substrate, temperature, and other experimental conditions: M. Busch, M. Schlageter, D. Weingand, T. Gehring, *Chem. Eur. J.* **2009**, *15*, 8251–8258.
[14] Y. Zhao, D. G. Truhlar, *Acc. Chem. Res.* **2008**, *41*, 157–167.
[15] The M05-2X functional implicitly accounts for "medium-range" electron correlation because of the way in which it is parametrized. This is sufficient to describe the dispersion interactions within many complexes, apart from hydrogen-bonded systems, in which much of the dispersion interaction is "long-range" (>5 Å). E. G. Hohenstein, S. T. Chill, C. D. Sherrill, *J. Chem. Theory Comput.* **2008**, *4*, 1996–2000.
[16] M. D. Wodrich, C. Corminboeuf, P. R. Schreiner, A. A. Fokin, P. von R. Schleyer, *Org. Lett.* **2007**, *9*, 1851–1854.
[17] a) E. A. Amin, D. G. Truhlar, *J. Chem. Theory Comput.* **2008**, *4*, 75–85; b) A. Sorkin, D. G. Truhlar, E. A. Amin, *J. Chem. Theory Comput.* **2009**, *5*, 1254–1265.
[18] a) Computational details, optimized geometries and energies obtained with the program Gaussian 03 are reported in the Supporting Information; b) Gaussian 03, Revision E.01, M. J. Frisch, G. W. Trucks, H. B. Schlegel, G. E. Scuseria, M. A. Robb, J. R. Cheeseman, J. A. Montgomery, Jr., T. Vreven, K. N. Kudin, J. C. Burant, J. M. Millam, S. S. Iyengar, J. Tomasi, V. Barone, B. Mennucci, M. Cossi, G. Scalmani, N. Rega, G. A. Petersson, H. Nakatsuji, M. Hada, M. Ehara, K. Toyota, R. Fukuda, J. Hasegawa, M. Ishida, T. Nakajima, Y. Honda, O. Kitao, H. Nakai, M. Klene, X. Li, J. E. Knox, H. P. Hratchian, J. B. Cross, V. Bakken, C. Adamo, J. Jaramillo, R. Gomperts, R. E. Stratmann, O. Yazyev, A. J. Austin, R. Cammi, C. Pomelli, J. W. Ochterski, P. Y. Ayala, K. Morokuma, G. A. Voth, P. Salvador, J. J. Dannenberg, V. G. Zakrzewski, S. Dapprich, A. D. Daniels, M. C. Strain, O. Farkas, D. K. Malick, A. D. Rabuck, K. Raghavachari, J. B. Foresman, J. V. Ortiz, Q. Cui, A. G. Baboul, S. Clifford, J. Cioslowski, B. B. Stefanov, G. Liu, A. Liashenko, P. Piskorz, I. Komaromi, R. L. Martin, D. J. Fox, T. Keith, M. A. Al-Laham, C. Y. Peng, A. Nanayakkara, M. Challacombe, P. M. W. Gill, B. Johnson, W. Chen, M. W. Wong, C. Gonzalez, J. A. Pople, Gaussian, Inc., Wallingford, CT, **2004**.
[19] This conclusion can be deduced by the observation of a second-order dependency of the reaction rate on the aldehyde concentration coupled with the observation of a relatively low free energy of activation.
[20] The B3LYP functional systematically underestimates reaction barrier heights, and is known to be inaccurate for interactions dominated by medium-range correlation energy, such as van der Waals attraction and aromatic–aromatic stacking. See reference [14], and references therein.
[21] J. Tomasi, B. Mennucci, R. Cammi, *Chem. Rev.* **2005**, *105*, 2999–3093.
[22] We previously considered only the complexes **6**-*R*,*anti-R*,*anti-P*, **6**-*R*,*anti-R*,*syn-P*, and **6**-*R*,*anti-S*,*anti-P* at the B3LYP/6–31G(d)//HF/3-21Gd level of theory.[10]
[23] We previously emphasized the greater steric interactions between isopropyl groups in the *syn* arrangement with respect to the *anti* arrangement.[10] In the light of the present results, this factor, although significant, cannot be considered the dominant one.
[24] In our previous study[10] we erroneously considered evolution of the complex **6**-*R*,*anti-S*,*anti-P* (Table 2, entry 10) as the most important catalytic cycle of the heterochiral dimer. Moreover, we did not succeed in locating the TS (**6**-*R*,*anti-R*,*syn-P*→**7**-*R*,*anti-RS*) at the HF/3-21Gd level of theory.

Received: September 15, 2009
Published online: January 29, 2010

